LETTER Communicated by Mike Arnold

Dynamical Working Memory and Timed Responses: The Role of Reverberating Loops in the Olivo-Cerebellar System

Werner M. Kistler
kistler@anat.fgg.eur.nl
Chris I. De Zeeuw
DeZeeuw@anat.fgg.eur.nl
Department of Neuroscience, Erasmus University Rotterdam, The Netherlands

This article explores dynamical properties of the olivo-cerebellar system that arise from the specific wiring of inferior olive (IO), cerebellar cortex, and deep cerebellar nuclei (DCN). We show that the irregularity observed in the firing pattern of the IO neurons is not necessarily produced by noise but can instead be the result of a purely deterministic network effect. We propose that this effect can serve as a dynamical working memory or as a neuronal clock with a characteristic timescale of about 100 ms that is determined by the slow calcium dynamics of IO and DCN neurons. This concept provides a novel explanation of how the cerebellum can solve timing tasks on a timescale that is two orders of magnitude longer than the millisecond timescale usually attributed to neuronal dynamics.

One of the key ingredients of our model is the observation that due to postinhibitory rebound, DCN neurons can be driven by GABAergic ("inhibitory") input from cerebellar Purkinje cells. Topographic projections from the DCN to the IO form a closed reverberating loop with an overall synaptic transmission delay of about 100 ms that is in resonance with the intrinsic oscillatory properties of the inferior olive.

We use a simple time-discrete model based on McCulloch-Pitts neurons in order to investigate in a first step some of the fundamental properties of a network with delayed reverberating projections. The macroscopic behavior is analyzed by means of a mean-field approximation. Numerical simulations, however, show that the microscopic dynamics has a surprisingly rich structure that does not show up in a mean-field description. We have thus performed extensive numerical experiments in order to quantify the ability of the network to serve as a dynamical working memory and its vulnerability by noise. In a second step, we develop a more realistic conductance-based network model of the inferior olive consisting of about 20 multicompartment neurons that are coupled by gap junctions and receive excitatory and inhibitory synaptic input via AMPA and GABAergic synapses. The simulations show that results for the time-discrete model hold true in a time-continuous description.

Neural Computation **14, 2597–2626** (2002)

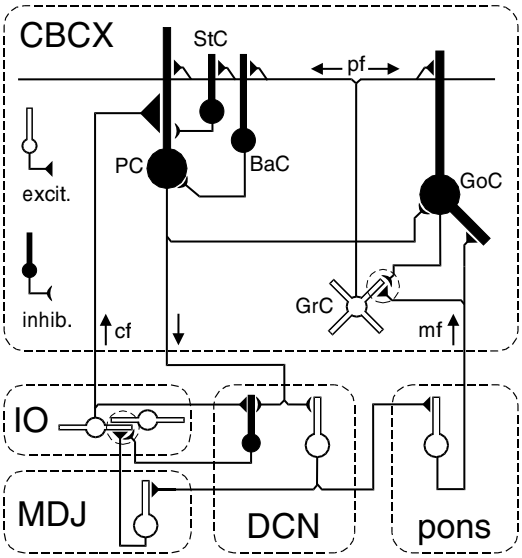

Figure 1: Schematic drawing of the cerebellar network. Excitatory and inhibitory neurons are shown as empty and filled circles, respectively. The following abbreviations are used. CBCX, cerebellar cortex; IO, inferior olive; MDJ, mesodiencephalic junction; DCN, deep cerebellar nuclei; PC, Purkinje cell; StC, stellate cell; BaC basket cell; GoC, Golgi cell; GrC, granule cell; pf, parallel fiber; cf, climbing fiber; mf, mossy fiber.

1 Introduction

From a morphological, a physiological, and a functional point of view, the inferior olive (IO) is a particularly interesting structure of the mammalian brain. The neurons of the IO are densely coupled by gap junctions (Sotelo, Llinás, & Baker, 1974); excitatory and inhibitory synapses meet each other in dendritic glomeruli located at the site of the gap junctions (De Zeeuw et al., 1998); slice recordings reveal subthreshold oscillations of the membrane potential (Llinás & Yarom, 1986); and, finally, the IO is the sole source of climbing fibers that control synaptic plasticity in cerebellar Purkinje cells (Szentagothai & Rajkovits, 1959; Desclin, 1974).

Cerebellar Purkinje cells (PCs) receive excitatory synaptic input from two different fiber systems: parallel fibers and climbing fibers (Ito, 1984). Each Purkinje cell receives input from up to 200,000 parallel fibers, the axons of the granule cells that relay information from the mossy fibers (see Figure 1). This massive input is contrasted by the input from a single climbing fiber that each Purkinje cell receives. While parallel fibers form only rather weak *en passant* synapses with PCs, climbing fibers literally climb up into the

dendritic tree of "their" PC and produce several synaptic transmission sites. The result is an extraordinarily strong synaptic coupling between climbing fiber and PC so that a single action potential in a climbing fiber is sufficient to trigger a sodium spike, followed by a short burst of spikelets in the corresponding PC. This so-called complex spike can easily be distinguished from "regular" simple spikes that are triggered by the parallel fiber input. The complex spike activity in the cerebellar cortex is thus a faithful image of the underlying IO activity.

Since the early 1970s, a lot of information about the electrophysiology of the olivo-cerebellar system has been collected. Climbing fibers deliver irregular trains of action potentials at a rather low rate of about one or two spikes per second. Multiple electrode recordings from the cerebellar cortex show that complex spikes in nearby PCs within a common microzone can be highly synchronized (Bell & Kawasaki, 1972; Llinás & Sasaki, 1989; Lang, Sugihara, Welsh, & Llinás, 1999; Lang, 2001). It is commonly accepted that this synchrony is (at least partially) due to the dense coupling of IO neurons by gap junctions (Sotelo et al., 1974; De Zeeuw et al., 1996, 1998).

Despite the irregular firing of individual IO neurons in vivo, IO neurons do have a tendency to fire rhythmically at a frequency of about 10 Hz. The intrinsic oscillatory properties of IO neurons are manifest in slice recordings where IO neurons show pronounced subthreshold oscillations of the membrane potential (Llinás & Yarom, 1986; Lampl & Yarom, 1993; Bal & McCormick, 1997). Autocorrelograms of the complex spike activity also show an oscillatory component at about 10 Hz that becomes very pronounced in the presence of tremorgenic drugs like harmalin or blockage of GABAergic synapses with picrotoxin (Llinás & Sasaki, 1989; Lang et al., 1999; Lang, 2001; Lang, Sugihara, & Llinás, 1996).

The above findings are readily taken into account by the time window model of IO activity (Kistler & van Hemmen, 1999; Kistler, van Hemmen, & De Zeeuw, 2000). In summary, the activity of IO neurons that innervate the same microzone is characterized by narrow time windows that encompass their potential firing times. Due to the oscillatory properties of IO neurons, there is a time window every 100 ms during which neurons can fire an action potential. Since the firing frequency of individual IO neurons is only about 1 Hz, each neuron fires on average only in 1 out of 10 time windows. Consequently, the population activity shows a 10 Hz oscillation with a high degree of synchrony, whereas individual neurons are firing irregularly at a much lower rate (see Figure 2).

The oscillatory component of the IO activity is not only due to intrinsic electrophysiological properties of IO neurons but can also be enhanced by the network in which the IO is embedded. Activity from the IO can reverberate back to the IO with a delay of about 100 ms, which matches the period of the intrinsic oscillation (Kistler & van Hemmen, 1999; Kistler et al., 2000). In short, complex spikes in cerebellar Purkinje cells are often followed by a pause in their simple spike activity (Armstrong, Cogdell, &

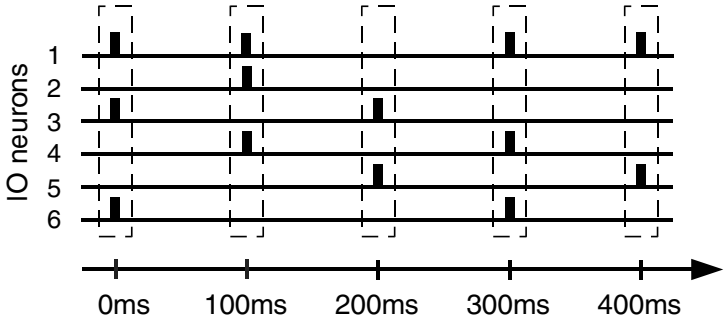

Figure 2: The time window hypothesis of inferior-olivary activity. IO neurons tend to fire action potentials during narrow time windows every 100 ms. Since the firing frequency of individual IO neurons is much lower than 10 Hz, they fire in only one out of about 10 windows. Spikes within each time window are highly synchronized.

Harvey, 1975, 1979; Loewenstein, Yarom, & Sompolinsky, 2000). During this pause, neurons from the deep cerebellar nuclei recover from the inhibition produced by the Purkinje cells and respond after a delay of about 100 ms with a short burst of rebound spikes (Jahnsen, 1986; Llinás & Mühlethaler, 1988; Ruigrok, 1997; Aizenman, Manis, & Linden, 1998; Aizenman & Linden, 1999; Czubayko, Sultan, Thier, & Schwarz, 2001). The rebound activity is conveyed by topographic projections from the DCN either directly or via the mesodiencephalic junction back to the IO (De Zeeuw & Ruigrok, 1994; De Zeeuw et al., 1998).[1] (See Figure 1.)

The aim of this article is to investigate the role of the resonant feedback the IO receives via delayed reverberating loops. In section 2, a simple mathematical model of networks with delayed reverberating projections is developed that gives some interesting insights into network dynamics and the role of divergence and convergence within the network. It turns out that the network can produce complex sequences of ever-differing firing patterns that look random but are completely determined by the wiring of the reverberating loop. Macroscopically, the dynamics is (in most cases) simply attracted by a fixed point for the population activity. Microscopically, however, the system exhibits a limit cycle behavior with numerous extremely large attractors, a behavior that has been studied to some extent in the context of spin-glass models (Kirkpatrick & Sherrington, 1978; Nützel, 1991) and attractor neural network models (Nützel, Kien, Bauer, Altman, & Krey,

[1] Note that the flocculus, which is projecting to the vestibular nuclei instead of the DCN, is not part of this reverberating loop (De Zeeuw, Wiley, Digiorgi, & Simpson, 1994). With *cerebellum* or *cerebellar*, we are thus referring primarily to the neocerebellum.

1994). We demonstrate by means of numerical experiments that even in the presence of noisy synaptic transmission failures, the microscopic dynamics is still partially determined by the topology of the reverberating loop. This observation, which goes beyond the more straightforward conclusion that reverberating loops can result in sustained network activity (Boylls, 1978; Crick, 1994; Billock, 1997), has interesting functional implications for working memory and timing tasks.

In section 3 we develop a conductance-based network model for a subpopulation of IO neurons. This model is used to validate the intrinsic assumptions of the time-discrete model, in particular, assumptions regarding synchrony and rhythmicity. The model also provides insight into the role of gap junctions in synchronization and spike timing. In the last section, we discuss functional implications and potential applications for working memory and timing tasks.

2 Networks with Delayed Reverberating Projections

In this section, we investigate the dynamical properties of neuronal networks that are part of a delayed reverberating loop. We assume that the delayed feedback is in resonance with the oscillation of the population activity and that the neurons stay synchronized, firing only during narrow time windows every T milliseconds. We furthermore assume that the set of neurons that is active in each cycle depends on only their current synaptic input that is due to the reverberating loop and thus depends only on the activity of the previous cycle. We employ a time-discrete description based on McCulloch-Pitts neurons. Each time step corresponds to one cycle of length T. The wiring of the reverberating loop is represented by a random coupling matrix. The statistical properties of the coupling matrix reflect the level of divergence and convergence within the reverberating network.

We introduce three models that differ slightly with respect to their treatment of inhibitory projections. In a first step, we derive mean-field equations for each of these models and discuss their macroscopic behavior. In a second step, we look more closely into the microscopic dynamics. It will turn out that subtle changes in the density of excitatory and inhibitory projections can have dramatic effects on the microscopic dynamics that do not show up in a mean-field description. Similar models have been studied in various contexts by Kirkpatrick and Sherrington (1978), Derrida, Gardner, & Zippelius, (1987), Crisanti and Sompolinsky (1988), Nützel (1991), and Kree and Zippelius (1991), to mention only a few.

2.1 Mean-Field Dynamics.

2.1.1 Excitatory Projections Only. We consider a population of N McCulloch-Pitts neurons (McCulloch and Pitts, 1943) that is described by a state vector $\boldsymbol{S} \in \{0, 1\}^N$. In each time step t_n, any given neuron i is either active

$[S_i(t_n) = 1]$ or inactive $[S_i(t_n) = 0]$. Due to the reverberating loop, neurons receive (excitatory) synaptic input h that depends on the wiring of the loop, described by a coupling matrix J, and on the activity during the previous cycle, that is,

$$h_i(t_n) = \sum_{j=1}^{N} J_{ij} S_j(t_{n-1}). \tag{2.1}$$

Since the wiring of the reverberating loop at the neuronal level is unknown, we adopt a random coupling matrix with binary entries. More precisely, we take all entries J_{ij} to be identically and independently distributed (i.i.d.) with

$$\text{prob}\{J_{ij} = 1\} = \lambda/N.$$

We thus neglect possible differences in the synaptic coupling strength and content ourself with a description that accounts only for the presence or absence of a projection. In that sense, λ is the convergence and divergence ratio of the network, that is, the averaged number of synapses that each neuron receives from and connects to other neurons, respectively.

The neurons are modeled as deterministic threshold elements. The dynamics is given by

$$S_i(t_n) = \Theta\left[h_i(t_n) - \vartheta\right], \tag{2.2}$$

with ϑ being the firing threshold and Θ the Heaviside step function with $\Theta(x) = 1$ if $x \geq 1$ and $\Theta(x) = 0$ for $x < 0$.

Starting with a random initial firing pattern,

$$S_i(t_0) \in \{0, 1\} \text{ i.i.d. with } \text{prob}\{S_i(t_0) = 1\} = a_0,$$

we can easily calculate the expectation value of the activity $a_1 = N^{-1} \sum_{i=1}^{N} S_i(t_1)$ in the next time step. According to equation 2.2, a neuron is active if it receives input from at least ϑ neurons that have been active during the last cycle. The initial firing pattern $\boldsymbol{S}(t_0)$ and the coupling matrix J are independent, so the synaptic input h in equation 2.1 follows a binomial distribution. The probability a_1 of any given neuron to be active in the next cycle is thus

$$a_1 = \sum_{k=\vartheta}^{N} \binom{N}{k} (a_0 \lambda N^{-1})^k (1 - a_0 \lambda N^{-1})^{N-k}. \tag{2.3}$$

This equation gives the network activity a_1 as a function of the activity a_0 in the previous cycle. It is tempting to generalize this expression so as to relate the activity a_n in cycle n recursively to the activity in cycle $n - 1$,

$$a_{n+1} = 1 - \sum_{k=0}^{\vartheta-1} \binom{N}{k} (a_n \lambda N^{-1})^k (1 - a_n \lambda N^{-1})^{N-k}. \tag{2.4}$$

Unfortunately, this is in general not possible because the activity pattern $\boldsymbol{S}$ in cycle $n \geq 1$ and the coupling matrix J are no longer independent, and correlations in the firing patterns can occur. For sparse networks with $\lambda \ll N$, however, these correlations can be neglected, and equation 2.4 can be used as an approximation (see Kree & Zippelius, 1991, for a precise definition of "$\lambda \ll N$"). Fortunately, the case with $\lambda \ll N$ is the more interesting one anyway, because otherwise, a_1 is a steep sigmoidal function of a_0, and the network activity either saturates ($a_1 \approx 1$) or dies out ($a_1 \approx 0$) after only one iteration. Furthermore, $\lambda \ll N$ is a realistic assumption for the reverberating loops of the olivo-cerebellar system. In the following, we thus assume that $\lambda \ll N$ so that the network activity is given by equation 2.4, or, if we approximate the binomial distribution by the corresponding Poisson distribution, by the recursion

$$a_{n+1} = 1 - \sum_{k=0}^{\vartheta-1} \frac{(a_n\lambda)^k}{k!}\, \mathrm{e}^{-a_n\lambda}. \tag{2.5}$$

The dynamics of the population activity is completely characterized by the mean-field equation, 2.5. For instance, it can easily be shown that $a_n = 0$ is a stable fixed point except if $\vartheta = 1$ and $\lambda > 1$. Furthermore, a_n is a monotonously growing function of a_{n-1}. Therefore, no macroscopic oscillations can be expected. In summary, three different constellations can be discerned (see Figure 3). First, for $\vartheta = 1$ and $\lambda > 1$, there is a stable fixed point at high levels of a_n; the fixed point at $a_n = 0$ is unstable. Second, if the firing threshold ϑ is large compared to the convergence λ, only $a_n = 0$ is stable. Finally, if $\vartheta > 1$ and λ are sufficiently large, bistability of $a_n = 0$ and $a_n > 0$ can be observed.

Figure 4 summarizes the dynamical properties of equation 2.5 for different combinations of the parameters ϑ and λ. As can be seen from the graphs, the fixed points of a_n are always rather rapidly reached, except for the few cases where the graph of $a_n(a_{n-1})$ is closely below the diagonal $a_n = a_{n-1}$, that is, for $\vartheta = 2$ and $\lambda = 3$. In this case, the dynamics approaches the fixed point at $a_n = 0$ in small steps after a large number of iterations (see Figure 3B).

2.1.2 Excitatory and Inhibitory Projections. Apart from excitatory reverberating projections via cerebellar cortex, deep cerebellar nuclei, and mesodiencephalic junction, there are also inhibitory projections from the deep cerebellar nuclei directly back to the inferior olive. All these projections are topographically organized so that both excitatory and inhibitory projections come simultaneously into play.

Our previous model can easily be extended so as to account for both excitatory and inhibitory projections. The wiring of the excitatory loop is

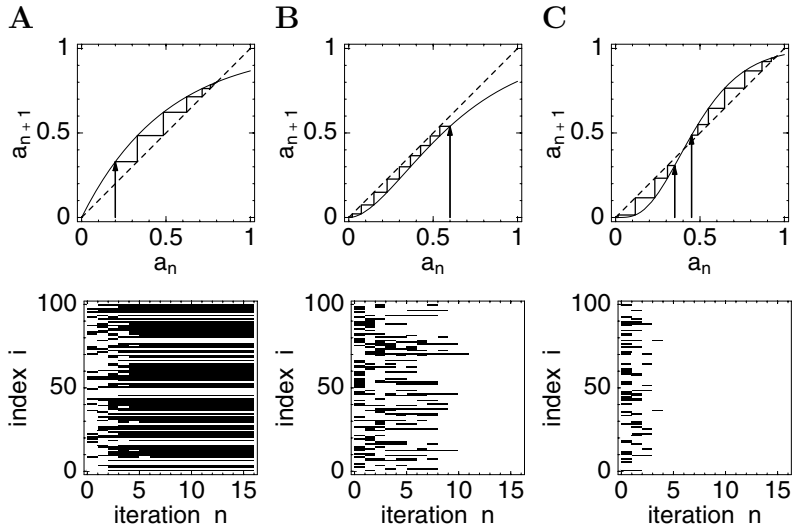

Figure 3: Dynamics of a reverberating loop with purely excitatory projections. The upper row shows the mean-field approximation of the population activity a_{n+1} as a function of the activity in the previous cycle a_n; see equation 2.5. The raster diagrams in the lower row give examples of the underlying microscopic dynamics in a simulation of $N = 100$ neurons. The time steps where a given neuron is active are marked by black bars. (A) $\lambda = 2$, $\vartheta = 1$: Stable fixed point at $a \approx 0.8$. (B) $\lambda = 3$, $\vartheta = 2$: Only $a_n = 0$ is stable. Note the long transient until the fixed point is reached. (C) $\lambda = 8$, $\vartheta = 4$: Bistability of $a_n = 0$ and $a_n \approx 0.95$.

characterized, as before, by a random matrix $J_{ij}^{\text{exc}} \in \{0, 1\}$ with

$$\text{prob}\{J_{ij}^{\text{exc}} = 1\} = \lambda_{\text{exc}}/N \qquad \text{i.i.d.}$$

Similarly, the wiring of the inhibitory loop is given by a random matrix $J_{ij}^{\text{inh}} \in \{0, 1\}$ with

$$\text{prob}\{J_{ij}^{\text{inh}} = 1\} = \lambda_{\text{inh}}/N \qquad \text{i.i.d.}$$

The parameters λ_{exc} and λ_{inh} describe the divergence or convergence of excitatory and inhibitory projections, respectively.

We assume that a neuron is activated if the difference between excitatory and inhibitory input exceeds its firing threshold ϑ. The dynamics is thus given by

$$S_i(t_n) = \Theta\left[\sum_{j=1}^{N} J_{ij}^{\text{exc}} S_j(t_{n-1}) - \sum_{j=1}^{N} J_{ij}^{\text{inh}} S_j(t_{n-1}) - \vartheta\right]. \tag{2.6}$$

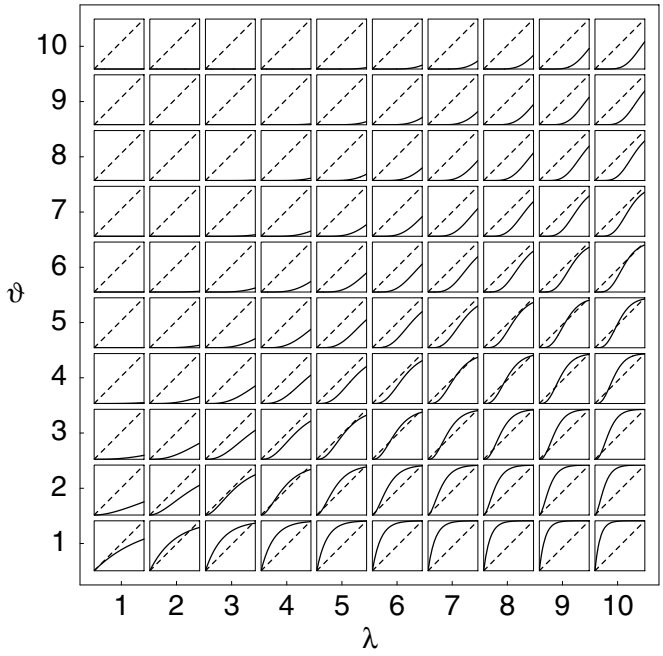

Figure 4: Overview of the mean-field behavior of a network with purely excitatory reverberating projections for various firing thresholds ϑ and projection densities λ. Each of the small diagrams within the table shows the activity a_n as a function of the activity a_{n-1} in the previous cycle. Axes range from 0 to 1.

As in the previous section, we can calculate the mean-field activity in cycle $n+1$ as a function of the activity in the previous cycle. We obtain

$$a_{n+1} = \sum_{k=\vartheta}^{N} \sum_{l=0}^{k-\vartheta} \frac{a_n^{k+l} \lambda_{\text{exc}}^{k} \lambda_{\text{inh}}^{l}}{k!l!} \, \mathrm{e}^{-a_n(\lambda_{\text{exc}}+\lambda_{\text{inh}})}. \tag{2.7}$$

The mean-field approximation is valid for sparse networks, that is, if $\lambda_{\text{exc}} \ll N$ and $\lambda_{\text{inh}} \ll N$.

As compared to the situation with purely excitatory feedback, equation 2.7 does not produce new modes of behavior. The only difference is that a_{n+1} is no longer a monotonous function of a_n. The slope $\mathrm{d}a_{n+1}/\mathrm{d}a_n$, however, cannot take values less than -1 so that macroscopic oscillations can be excluded (see Figures 5 and 6).

2.1.3 Shunting Inhibition. In the previous section, we implicitly assumed that excitatory and inhibitory synapses are equally strong and that excitatory and inhibitory input interact linearly. In reality, however, the reversal

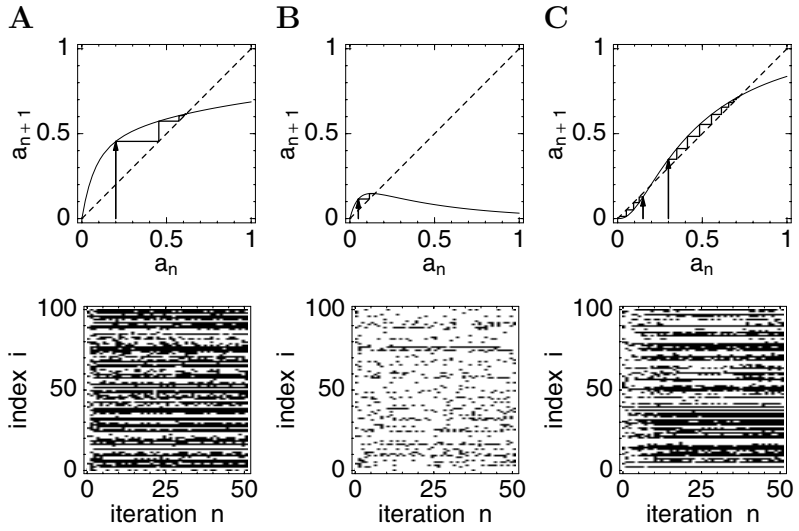

Figure 5: Dynamics of a reverberating loop with excitatory and inhibitory projections (similar plots as in Figure 3; see equations 2.6 and 2.7). (A) $\lambda_{exc} = 6$, $\lambda_{inh} = 4$, $\vartheta = 1$: Stable fixed point at $a_n \approx 0.6$. (B) $\lambda_{exc} = 4$, $\lambda_{inh} = 10$, $\vartheta = 1$: Stable fixed point at $a_n \approx 0.15$. (C) $\lambda_{exc} = 10$, $\lambda_{inh} = 4$, $\vartheta = 3$: Bistability between $a_n = 0$ and $a_n \approx 0.73$. Note the high level of irregularity in the raster diagrams. Although the mean-field dynamics is characterized by a simple fixed point, the corresponding limit cycle of the microscopic dynamics can have an extremely long period.

potential of inhibitory synapses is usually close to the resting potential of the neuron. The effect of activating an inhibitory synapse is therefore rather an increase of the membrane conductance than a lowering of the membrane potential. In addition, inhibitory synapses are often located directly at the soma so that the activity of the neuron is virtually shunted by inhibitory input.

We can easily modify equation 2.6 so as to mimic the different mechanisms of excitation and inhibition. Instead of using a subtractive interaction, we now write

$$S_i(t_n) = \Theta\left[\sum_{j=1}^{N} J_{ij}^{\text{exc}} S_j(t_{n-1}) - \vartheta\right] \Theta\left[-\sum_{j=1}^{N} J_{ij}^{\text{inh}} S_j(t_{n-1})\right]. \tag{2.8}$$

Thus, a neuron is active in cycle n if it receives at least ϑ action potentials via excitatory synapses and no inhibitory input. A single inhibitory presynaptic neuron is sufficient to shunt the neuron.

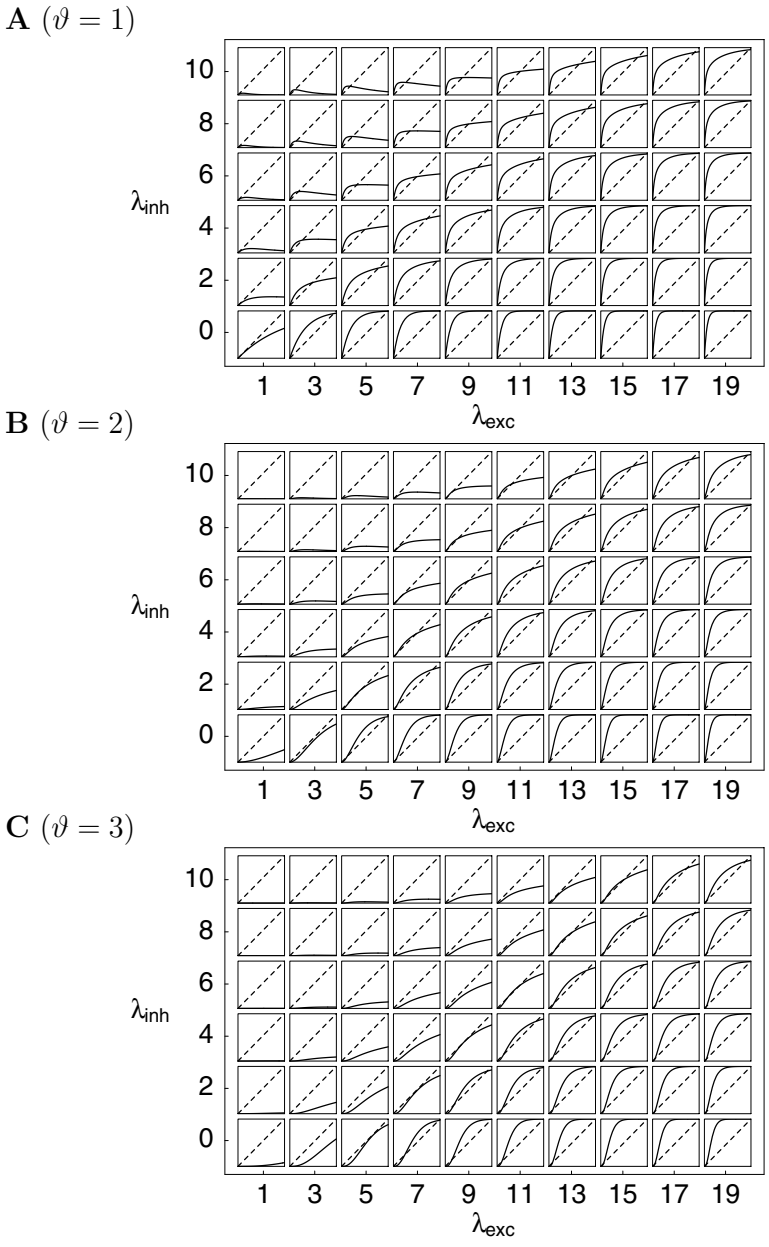

Figure 6: Overview of the mean-field behavior of a network with both excitatory and inhibitory reverberating projections. (A) Similar plots as in Figure 4 for $\vartheta = 1$ and various projection densities of excitatory (λ_{exc}) and inhibitory (λ_{exc}) projections. (B) Same as in *A* but $\vartheta = 2$. (C) $\vartheta = 4$. Axes range from 0 to 1.

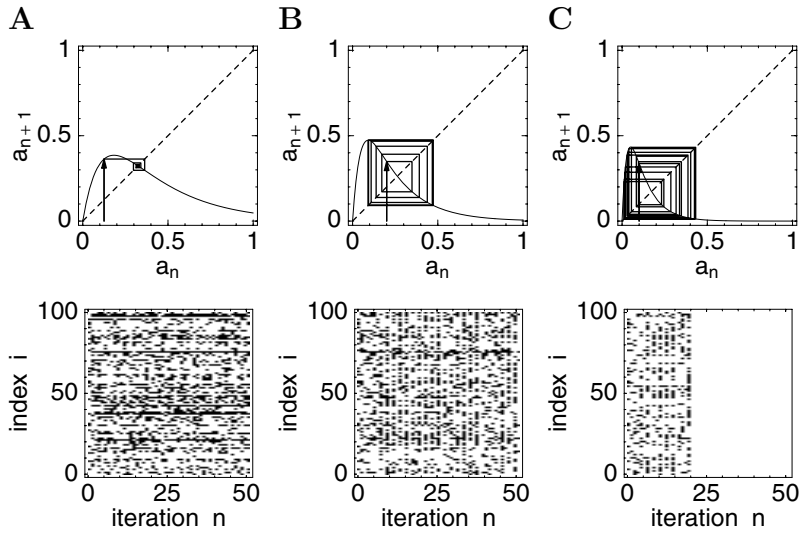

Figure 7: Dynamics of a reverberating loop with shunting inhibition (similar plots as in Figure 3; see equations 2.8 and 2.9). (A) $\lambda^{\mathrm{exc}} = 6$, $\lambda^{\mathrm{inh}} = 3$, $\vartheta = 1$: Fixed point at $a \approx 0.35$. (B) $\lambda^{\mathrm{exc}} = 15$, $\lambda^{\mathrm{inh}} = 5$, $\vartheta = 1$: Macroscopic oscillation of the population activity. The oscillations are also clearly visible in the simulation shown in the raster diagram. (C) $\lambda^{\mathrm{exc}} = 25$, $\lambda^{\mathrm{inh}} = 10$, $\vartheta = 1$: Chaotic behavior. Note that the activity in the simulation suddenly dies out at $n = 20$, which is due to the finite size of the network.

Since excitatory and inhibitory coupling matrices are independent, the mean-field activity is given by

$$a_{n+1} = \left[1 - \sum_{k=0}^{\vartheta-1} \frac{(a_n \lambda_{\mathrm{exc}})^k}{k!} \, \mathrm{e}^{-a_n \lambda_{\mathrm{exc}}}\right] \mathrm{e}^{-a_n \lambda_{\mathrm{inh}}}. \tag{2.9}$$

As compared to the situation with subtractive inhibition or with purely excitatory feedback, equation 2.9 has a richer dynamical structure (see Figure 7). Most notably, a_{n+1} is no longer a monotonous function of a_n, and the slope $\mathrm{d}a_{n+1}/\mathrm{d}a_n$ can take values less than -1 so that oscillations and even chaotic behavior can be observed (see Figures 8 and 9).

2.2 Microscopic Dynamics. As it is already apparent from the examples shown in Figures 3, 5, and 7, the irregularity of the spike trains produced by different reverberating loops can be quite different. Numerical experiments have shown that in the case of purely excitatory projections, fixed points of the mean-field dynamics almost always correspond to a fixed point of the microscopic dynamics, or at least to a limit cycle with short period. As soon

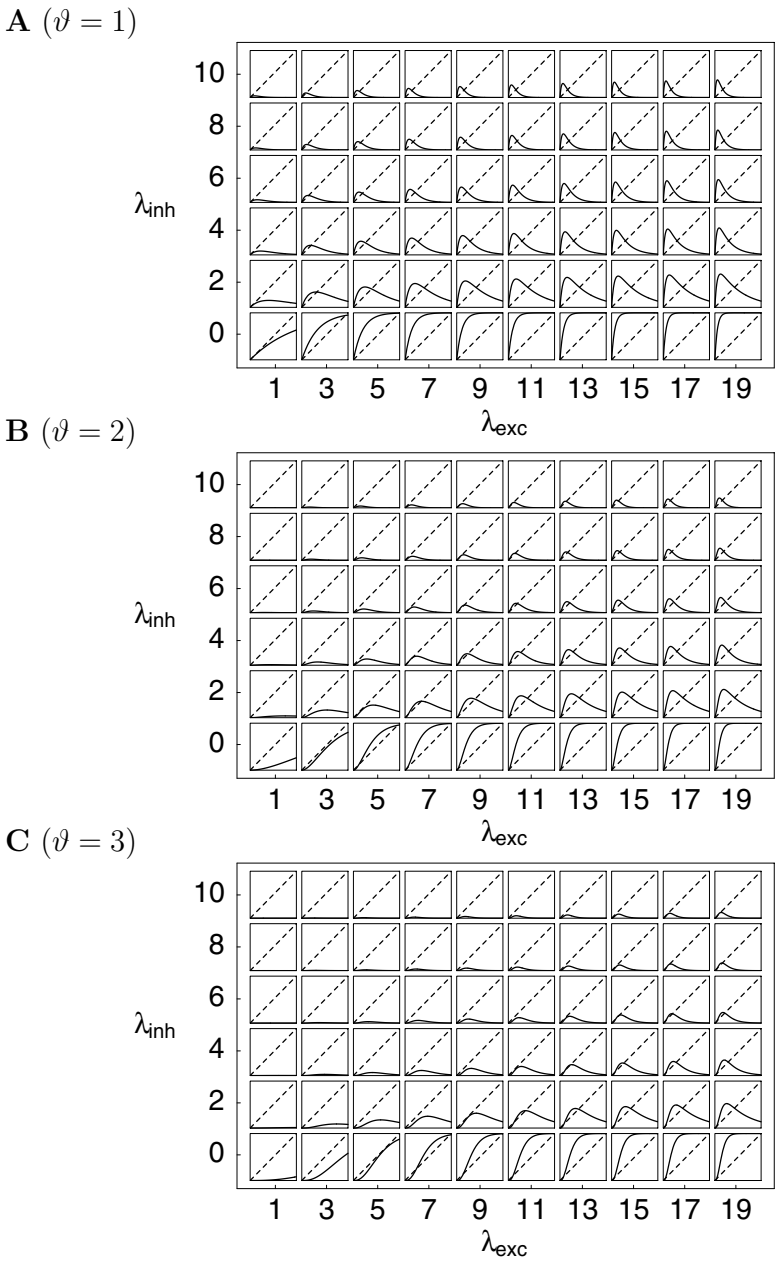

Figure 8: Similar plots as in Figure 6 but for shunting instead of subtractive inhibition.

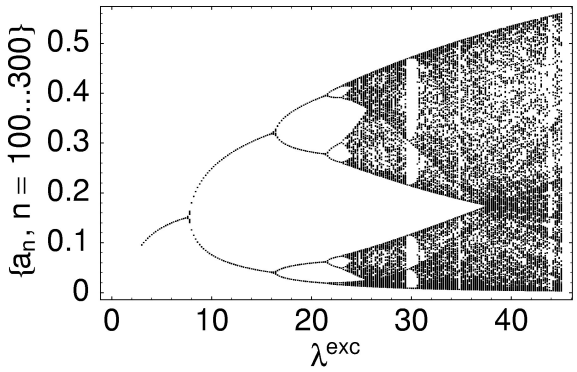

Figure 9: Bifurcation diagram of the mean-field activity in a reverberating network with shunting inhibition; see equation 2.9. A classical period-doubling scenario leads to chaotic behavior as the density of the excitatory projections λ_{exc} is increased. The density of the inhibitory projections $\lambda_{inh} = 10$ and the firing threshold $\vartheta = 1$ are kept constant.

as inhibitory projections are introduced, this situation changes dramatically. Fixed points in the mean-field dynamics still correspond to limit cycles in the microscopic dynamics; the length of the periods, however, is substantially larger and grows rapidly with the network size. A similar phenomenon was observed in a spin-glass model with random gaussian couplings (Nützel, 1991).

We have performed numerical experiments in order to quantify the dependency of the attractor size on the network architecture. Figure 10 A shows the period of the microscopic limit cycle averaged over 100 realizations of the network and the initial firing pattern as a function of the density of inhibitory projections. Starting by a period of 1 for $\lambda_{inh} = 0$, the averaged period quickly rises to very large values depending on the actual network size. For small networks, the probability of ending up in the all-off fixed point increases to significant levels as the density of the inhibitory projections exceeds 3 or 4. Therefore, the averaged length of the limit cycle drops back to 1 as λ_{inh} increases even further. There is a large variability in the length of the attractors produced by different realizations of the network or that are reached from different initial patterns in the same network. Figure 10B exhibits the maximum period length encountered in 100 randomly chosen realizations of network and initial pattern. The maximal values are about one order of magnitude larger than the mean.

With respect to potential applications, it is particularly interesting to see how information about the initial firing pattern is preserved in the sequence of patterns generated by the reverberating network. To this end, we have generated random initial patterns $\boldsymbol{S}_0$ and estimated the transinformation

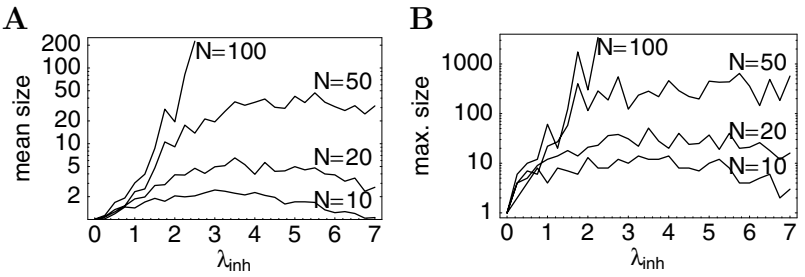

Figure 10: Attractor length as a function of the inhibitory projection density λ_{inh} and the network size $N = 10, 20, 50, 100$. (A) Length of the attractor averaged over 100 realizations of the coupling matrices and the initial pattern. The density of excitatory projections is kept constant at $\lambda_{\text{exc}} = 3$; the firing threshold is $\vartheta = 1$. The dynamics (subtractive inhibition) is given by equation 2.6. (B) Maximal length of the attractor of 100 randomly chosen realizations of coupling matrices and initial patterns. Comparison of *A* and *B* shows that there is a large variability in the actual attractor length.

$I(\boldsymbol{S}_0, \boldsymbol{S}_n)$ between the initial pattern and the pattern $\boldsymbol{S}_n$ generated by n iterations,

$$I(\boldsymbol{S}_0, \boldsymbol{S}_n) = H(\boldsymbol{S}_n) - H(\boldsymbol{S}_n \mid \boldsymbol{S}_0), \tag{2.10}$$

with $H(\boldsymbol{S}_n)$ being the entropy of a random variable $\boldsymbol{S}_n$ and $H(\boldsymbol{S}_n \mid \boldsymbol{S}_0)$ the conditional entropy of $\boldsymbol{S}_n$ given $\boldsymbol{S}_0$. Recall that the entropy of a random variable x with realizations $x_1, x_2, \ldots$ and probability distribution $\text{prob}\{x_i\}$ is defined as

$$H(x) = -\sum_i \text{prob}\{x_i\} \log_2(\text{prob}\{x_i\}). \tag{2.11}$$

Similarly, the conditional entropy $H(x \mid y)$ of x given y is (Ash, 1990),

$$H(x \mid y) = -\sum_{i,j} \text{prob}\{x_i, y_j\} \log_2(\text{prob}\{x_i \mid y_j\}). \tag{2.12}$$

Figure 11 shows numerical results for the transinformation $I(\boldsymbol{S}_0, \boldsymbol{S}_n)$ obtained for small networks ($N \in \{16, 20\}$) with subtractive or shunting inhibition averaged over 10 different realizations of the coupling matrices. We have paid particular attention not to overestimate the transinformation by using a sufficiently large number of samples (up to $n_{\text{samples}} = 500{,}000$ randomly chosen initial conditions per network) and extrapolating the results to $n_{\text{samples}} \to \infty$ (Treves & Panzeri, 1995). We found that the transinformation decays within the first few iterations from the maximal value

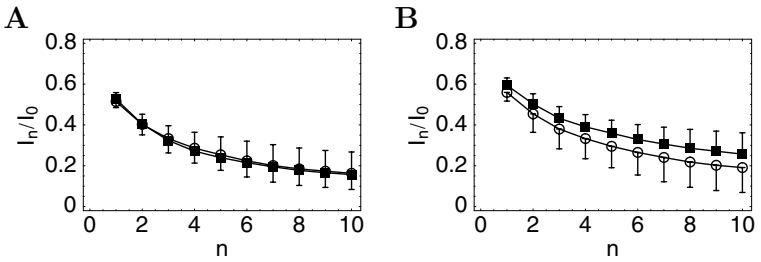

Figure 11: Preservation of information about the initial firing pattern in a reverberating loop with $N = 16$ (open circles) and $N = 20$ (filled squares) neurons. The transinformation $I(S_0, S_n)$ between the initial pattern and the pattern after n iterations is normalized by the maximum $I(S_0, S_0)$. Error bars give the standard deviation of 10 different realizations of the coupling matrices. (A) Subtractive inhibition with $\lambda_{\text{exc}} = 5$, $\lambda_{\text{inh}} = 5$, $\vartheta = 1$; see equation 2.6. (B) Shunting inhibition with $\lambda_{\text{exc}} = 6$, $\lambda_{\text{inh}} = 3$, $\vartheta = 1$; see equation 2.8.

$I_0 = I(\boldsymbol{S}_0, \boldsymbol{S}_0)$ to about $0.2I_0$. The initial decay reflects the length of the transient until the limit cycle is reached. The asymptotic value of $I(\boldsymbol{S}_0, \boldsymbol{S}_n)$ as $n \to \infty$ depends on the averaged number of initial patterns that end up on the same limit cycle.

Once the state of the network has reached a limit cycle, it will stay there forever due to the purely deterministic dynamics given by equations 2.2, 2.6, or 2.8. In reality, however, the presence of noise leads to mixing in the phase-space so that the information about the initial state will finally be lost. There are several sources of noise in a biological network. The most prominent are uncorrelated noisy synaptic input from other neurons and synaptic noise caused by synaptic transmission failures. In order to investigate the impact of noise on the preservation of information in the reverberating network, we have repeated the calculation of transinformation for a network with synaptic noise, that is, a network where synaptic transmission fails with a certain probability p_{fail}. More precisely, we determined for each neuron the number of spikes $h_i^{\text{exc}}(t_n) = \sum_j J_{ij}^{\text{exc}} S_j(t_{n-1})$ a neuron would receive without noise via excitatory synapses and subtracted from this number a random number k_i^{exc} drawn from a binomial distribution with parameters $\mathcal{N} = h_i^{\text{exc}}(t_n)$ (number of trials) and $p = p_{\text{fail}}$ (probability of success per trial). The same was done (independently) for inhibitory input. The thus reduced amount of input was then plugged into the dynamical equation. In case of subtractive inhibition, the above procedure gives

$$S_i(t_n) = \Theta\left[\sum_{j=1}^{N} J_{ij}^{\text{exc}} S_j(t_{n-1}) - \sum_{j=1}^{N} J_{ij}^{\text{inh}} S_j(t_{n-1}) - k_i^{\text{exc}} + k_i^{\text{inh}} - \vartheta\right]. \qquad (2.13)$$

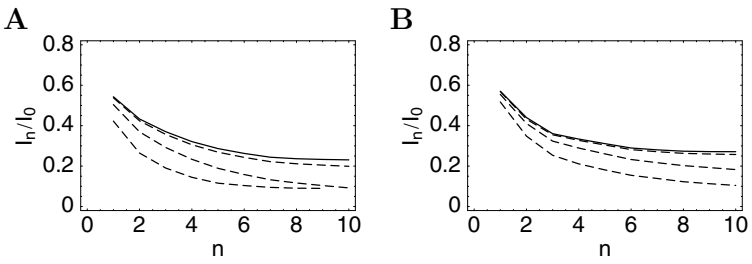

Figure 12: Preservation of information about the initial pattern in a reverberating network with synaptic noise. The solid line is the noise-free reference ($p_{\text{fail}} = 0$), the dashed lines correspond to $p_{\text{fail}} = 0.001$, $p_{\text{fail}} = 0.01$, and $p_{\text{fail}} = 0.05$ (from top to bottom). (A) Subtractive inhibition with $N = 16$, $\lambda_{\text{exc}} = 5$, $\lambda_{\text{inh}} = 5$, $\vartheta = 1$; see equation 2.6. (B) Shunting inhibition with $N = 16$, $\lambda_{\text{exc}} = 6$, $\lambda_{\text{inh}} = 3$, $\vartheta = 1$; see equation 2.8.

Figure 12 shows the amount of information about the initial pattern that is left after n iterations in the presence of synaptic noise in a small network with $N = 16$ neurons. As expected, unreliable synapses lead to a faster decay of the initial information. A failure probability of 5% already leads to a significantly reduced capacity. We discuss the role of synaptic reliability more extensively in section 4.

3 A Model of the Inferior Olive

We have seen that a simple time-discrete model of a delayed reverberating loop can produce complex sequences of ever-differing spike patterns. This model can provide an explanation for the experimentally observed irregularity of complex spikes. Due to the deterministic origin of the spike patterns, there may also be interesting functional implications for working memory and timing tasks.

In order to check whether the properties of the time-discrete description carry over to a model continuous in time, we have built a conductance-based model of a subpopulation of neurons from the inferior olive. The model is based on a two-compartment model of inferior olivary neurons developed by Schweighofer, Doya, and Kawato (1999). The simulations comprise up to 20 neurons coupled by gap junctions in an all-to-all fashion. Each neuron receives excitatory and inhibitory input via time-dependent conductances that mimic GABA and AMPA-sensitive synapses. In IO neurons, gap junctions, and excitatory and inhibitory synapses are tightly packed together in glomeruli located on distal dendrites (De Zeeuw et al., 1998). Therefore, the original IO model has been extended by an extra dendritic compartment that contains the synaptic conductances together with the gap junctions.

Each neuron thus consists of three compartments: a somatic compartment, a large dendritic compartment that represents the dendritic tree, and the extra compartment that mimics a single dendrite.

Delayed reverberating projections have been implemented phenomenologically by the activation of synaptic conductances with a delay of about 100 ms after the occurrence of an action potential in one of the IO neurons. Since the excitatory reverberating loop via the mesodiencephalic junction contains one more synaptic transmission than the inhibitory loop, the overall delay of the excitatory projections is 5 ms longer than the inhibitory loop. The topology of both reverberating loops is described once more by means of sparse random matrices (see the appendix for details).

Figure 13 shows an example of a simulation of the IO network. The initially silent network has been stimulated by a short depolarizing current pulse delivered to neurons 1 through 5. Due to the reverberating projections, this results in sustained activity in the form of irregular spike trains in each individual neuron; the population activity, however, shows a clear 10 Hz oscillation. Coupling by gap junctions and common synaptic input ensures that neurons that fire an action potential within a certain cycle remain synchronized despite the heterogeneity in the network (some neurons receive more excitatory input spikes than others and thus tend to fire earlier). The mechanisms underlying synchronization by synaptic and electrical coupling are well understood and described elsewhere (Gerstner, van Hemmen, & Cowan, 1996; Chow & Kopell, 2000).

The simulation shows that the central assumption of the time-discrete model is indeed justified; neurons firing within one cycle do stay synchronized. Moreover, the conductance-based model generates, after appropriate tuning of the synaptic conductances, the very same sequence of spike patterns as the simple time-discrete model. Figures 13B and 13C show a spike raster diagram for the conductance-based model and the corresponding time-discrete model with $\vartheta = 1$, respectively. Since there is perfect agreement, the spike patterns observed in the conductance-based model are solely determined by the topology of the excitatory and inhibitory reverberating loops.

It is interesting to check whether the correspondence between the two types of model holds true also for other configurations, for example, for other values of the firing threshold. Since the firing threshold cannot be directly accessed in conductance-based models, we have reduced the synaptic conductances in order to increase the amount of synaptic input required to trigger a spike. Figure 14 shows the results. The time-discrete model with $\vartheta = 2$ predicts that the activity dies out within four iterations. Again, there is perfect agreement between both models on the level of individual spikes.

Although postinhibitory rebound in DCN neurons seems to be a robust mechanism to trigger action potentials with a delay of about 100 ms (Kistler & van Hemmen, 1999; Kistler et al., 2000), there will always be a certain jitter

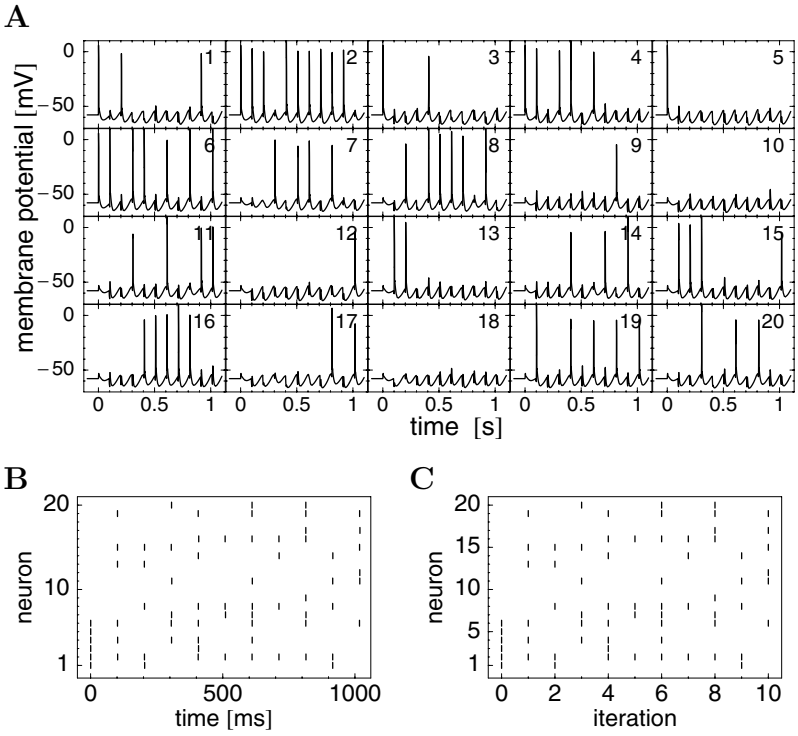

Figure 13: Simulation of a network of 20 IO neurons embedded in a reverberating loop with $\lambda_{\text{exc}} = 6$ and $\lambda_{\text{inh}} = 3$. (A) Membrane potentials as a function of time. The simulation was started by a short depolarizing current pulse in neurons 1–5 at time $t = 0$. (The number of the neurons is given in the upper-right corner of each graph.) The strength of the excitatory and inhibitory synapses is $g_{\text{AMPA}} = 8$ nS and $g_{\text{GABA}} = 18$ nS, respectively. (B) Spike raster diagram of the same simulation as in *A*. (C) Sequence of spike patterns as predicted by the time-discrete model, equation 2.8, with $\vartheta = 1$ for this specific choice of the coupling matrices. Comparison with *B* shows perfect agreement.

in the arrival time of the reverberated spike activity. Postsynaptic AMPA receptors have rather low time constants of a few milliseconds so that the amplitude of the overall postsynaptic potential triggered by a volley of incoming spikes can depend sensitively on the temporal dispersion of the volley. In the present context, for instance, activation of several excitatory synapses can fail to trigger the neuron if the temporal spread is too large. Furthermore, inhibitory spikes can prevent the triggering of an action potential only if they arrive before the excitatory volley. Any variability in the spike timing thus translates in noise in the amplitude of the postsynaptic

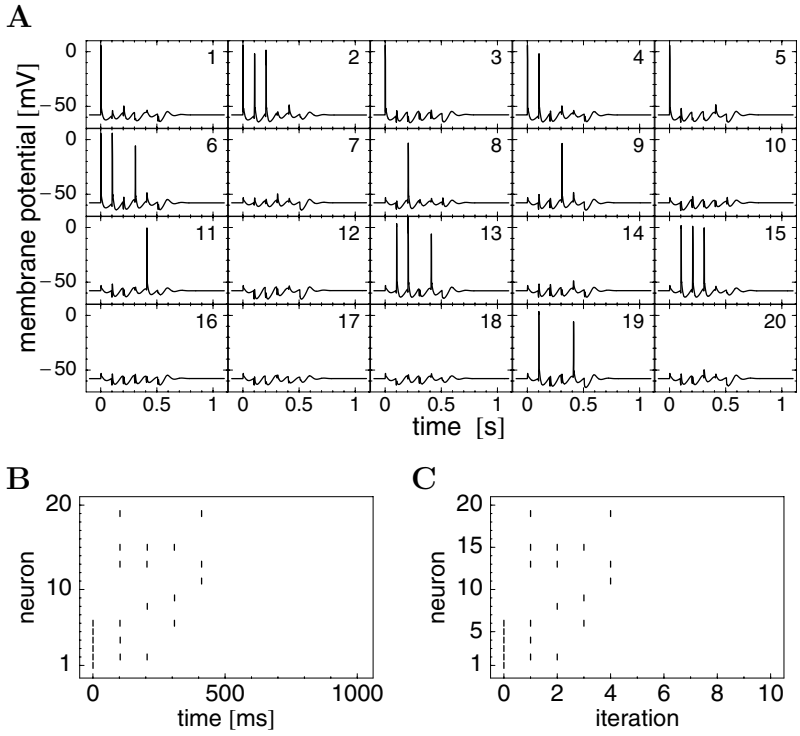

Figure 14: (A) Similar simulation as in Figure 13 but with weaker synapses ($g_{\mathrm{AMPA}} = 5$ nS and $g_{\mathrm{GABA}} = 12$ nS). The initial activity thus dies after a few cycles. (B) Corresponding spike raster diagram. (C) Spike pattern predicted by the time-discrete model, equation 2.8, with $\vartheta = 2$. As in Figure 13, there is perfect agreement between *B* and *C*.

potentials similar to the noise produced by synaptic transmission failures discussed in section 2.2.

A precise synchronization of IO neurons is thus essential in order to keep the dynamical working memory operational. In fact, multielectrode recordings have shown that complex spikes in nearby Purkinje cells can be synchronized on a millisecond timescale (Bell & Kawasaki, 1972; Llinás & Sasaki, 1989; Lang et al., 1999), a remarkable observation that usually is attributed to the gap junctional coupling of IO neurons. Recently, the role of gap junctions became experimentally accessible in genetically modified mice that are deficient of a certain protein (connexin36) that is part of gap junctions connecting cortical neurons (Rash et al., 2000; Güldenagel et al., 2001; Deans, Gibson, Sellitto, Connors, & Paul, 2001; Hormuzdi et al., 2001). Forthcoming experimental results on the degree of synchrony of complex

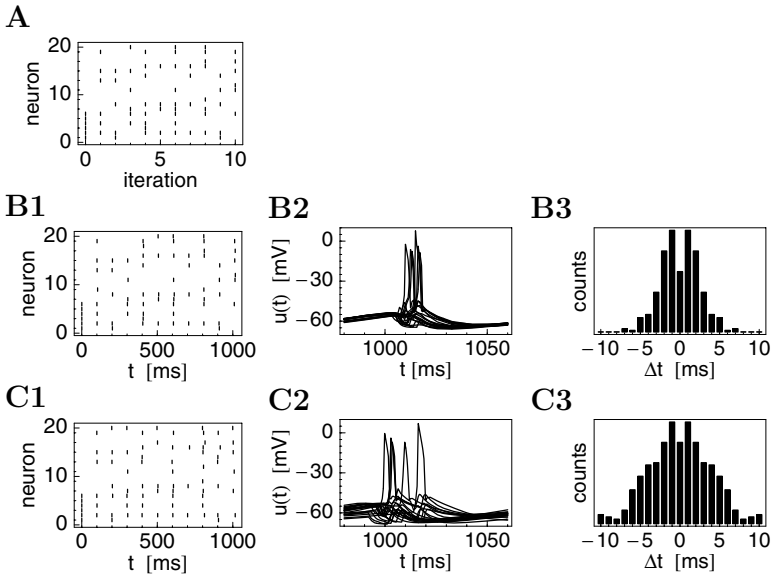

Figure 15: Similar simulation as in Figure 13 but with nonuniform delays of the reverberating projections. (A) Spike pattern predicted by the time-discrete model, equation 2.8. (B) Results of the corresponding simulation of the conductance-based IO model. (B1) Spike raster. Note that there are some discrepancies between $A1$ and $B1$ but both simulations finally reach the same attractor. (B2) Close-up of the spikes near $t = 1010$ ms. The jitter in the firing time is mostly due to the nonuniform delays of the reverberating projections. (B3) Autocorrelation of the population activity. The width of the peak is a measure for the degree of synchrony within each cycle. (C) Same simulation as in B but without gap junctions ($g_c = 0$). Compared to the time-discrete model, the spike raster (C1) shows several deviations that are due to the reduced level of synchrony within each cycle; see the spike train in $C2$ and the autocorrelogram in $C3$.

spike in these mice can be compared directly to simulations where gap junctions have been switched off by setting their conductance to zero.

Figure 15 shows an example of a simulation with noise in the timing of the reverberated spikes in the presence and absence of gap junctional coupling between IO neurons. The uniform delay of the reverberating projections has been replaced by a 6 ms wide distribution of delays. Comparison of the spike pattern generated by the time-discrete model in Figure 15A and the result from the conductance-based network model *with* gap junctions in Figure 15B shows a few missing and misplaced spikes near $t = 300, 400$, and 500 ms. Interestingly, however, the spike patterns at $t = 600, \ldots, 1000$ ms are again identical. If the gap junctions are switched off ($g_c = 0$), then significant

deviations in the spike patterns are apparent. Nevertheless, the synchrony of spikes within one cycle does not break down. The width of the peaks in the autocorrelation of the population activity is merely about twice as large as in the presence of gap junctions (see Figure 15C).

4 Discussion

The conclusions that can be drawn are twofold. First, purely deterministic mechanisms can generate irregular spike trains. Second, these spike trains can carry information about the initial pattern and the elapsed time even in the presence of noise.

We have studied this phenomenon for a concrete biological substrate, the olivo-cerebellar system. Activity from the IO triggers complex spikes in cerebellar Purkinje cells followed by a pause in the simple spike activity, which gives rise to a burst of rebound spikes in the cerebellar nuclei with a delay of about 100 ms. The rebound activity can reverberate back to the IO either directly via inhibitory projections or indirectly via excitatory neurons of the mesodiencephalic junction. The delayed reverberation is in resonance with the intrinsic oscillatory properties of the IO neurons. The activity of the IO is characterized by a periodic arrangement of narrow time windows that encompass potential firing times. The set of neurons active during one of these time windows determines due to the reverberating loop the set of neurons that fire a spike in the next time window.

Given the distinct firing characteristics of the IO neurons, a time-discrete model based on McCulloch-Pitts neurons with parallel dynamics is the natural choice. In this model, each time step of 100 ms corresponds to one cycle of the oscillating population activity. The corresponding mean-field dynamics can easily be solved and describes the macroscopic behavior as a function of the firing threshold and the divergence or convergence of the reverberating loops.

Although the macroscopic dynamics is mostly characterized by a simple fixed-point behavior, the microscopic dynamics can be very complex. Numerical experiments show that the period of the microscopic attractors corresponding to a fixed point of the population activity can be extremely long (Nützel, 1991). This has interesting implications for a long-standing discussion on the origin of the experimentally observed irregularity of neuronal activity—and, to our knowledge, the first explanation for the irregularity of the complex spike activity in Purkinje cells. It has been argued that neurons that integrate synaptic input from many presynaptic neurons cannot produce irregular spike trains unless the membrane time constant is unrealistically short or the presynaptic activity contains fluctuations with an amplitude that is comparable to the mean input (Softky & Koch, 1993; Shadlen & Newsome, 1994). The latter condition can be met by balancing the amount of excitation and inhibition that can be achieved in a sparse recurrent network without fine-tuning of parameters (van Vreeswijk & Sompolinsky,

1998; Brunel, 2000). This work demonstrates most clearly that the quenched noise in the random couplings of a sparse network is indeed capable of producing highly irregular spike trains without any additional sources of noise. Similar results have been obtained experimentally by Fusi, Del Giudice, & Amit (2000) with a hardware implementation of a recurrent network.

It is a priori impossible to decide whether the irregularity in neuronal spike trains is a result of noisy neurons and synapses or whether the irregularity is the signature of a highly efficient temporal code similar to the noise produced by a computer modem. The second conclusion, which is intimately related to the first one, does not provide the ultimate answer to this question but demonstrates that there is a solution in the middle: that the spike trains contain information, for example, on the initial firing pattern and the elapsed time even in the presence of (synaptic) noise. The reverberating network preserves this information for a certain amount of time depending on the level of noise. This is an emergent property of reverberating networks that is closely related to their chaotic microscopic dynamics. In an asynchronous network with balanced excitation and inhibition, two initially nearby states will diverge rapidly (van Vreeswijk & Sompolinsky, 1998). In the olivo-cerebella system, these states will also diverge, but this takes at least a few iterations. Due to the delayed triggering of spikes via postinhibitory rebound, each iteration corresponds to about 100 ms. The timescale on which information is lost is thus long enough to provide a useful storage device for past input. Similar to the idea of a liquid state machine (Maass, Natschläger, & Markram, in press), readout neurons can use this information for all sorts of real-time computation.

As a concrete example, we want to show that conclusion 2 provides a novel mechanism for the implementation of a working memory and the solution of timing tasks. Suppose that external (sensory) events trigger activity in certain subsets of neurons that are part of the reverberating loop. Different events trigger different neurons, therewith starting transients that end up in different attractors. The spike patterns thus represent simultaneously information about what happened and when it happened. The "what" information is implicitly stored by the attractor that is finally reached and "when" information is contained in the actual position of the network on the attractor or the transient leading to the attractor (see Figure 16). The network can hence serve as a working memory for external events. Note that this mechanism—in contrast to traditional attractor neural networks (Hopfield, 1982; Amit, 1989)—does not rely on any form of synaptic plasticity though synaptic plasticity, might help to stabilize certain transients and their attractors.

The critical question in this context is the vulnerability of the system by noise. In section 2.2, we saw that even a low failure rate of the synaptic transmission impairs the preservation of information from one cycle to the next. Nevertheless, a failure rate of 5% leaves after five iterations more than 10% of the information about the initial pattern (see Figure 12). This means

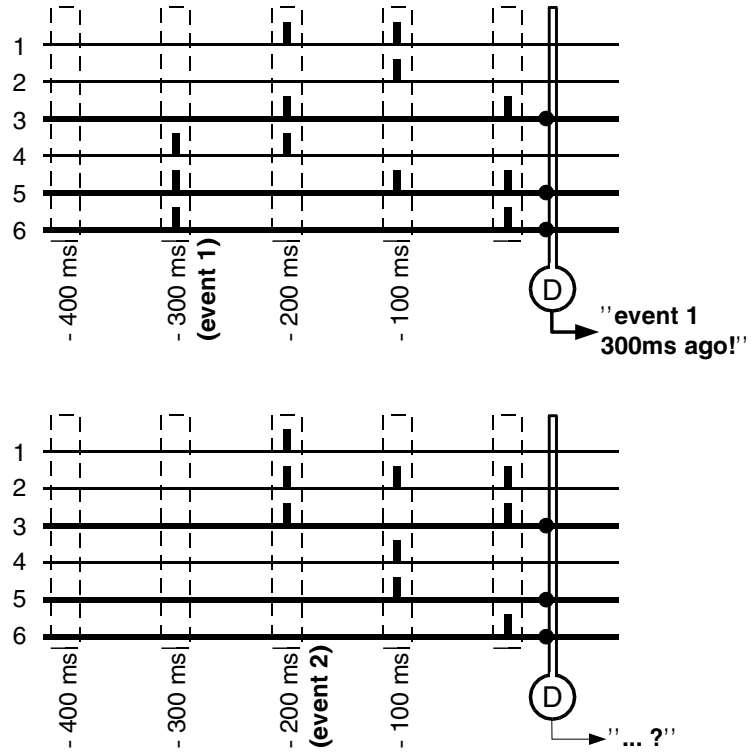

Figure 16: Simultaneous representation of "what" and "when" information. An external event (event 1) triggers a subset of neurons (4, 5, and 6) leading to a certain sequence of spike patterns. A detector neuron (D) from a superordinated layer can easily be trained to recognize a particular pattern from this sequence, for example, the pattern that occurs exclusively 300 ms after event 1 (upper diagram). Other events trigger a different sequence of spike patterns that do not trigger the detector neuron (lower diagram).

that 10 neurons are enough to discern two different events half a second after they actually occurred. Conditioning experiments where test animals are trained to react with a certain delay to a visual or auditory cue show that this is indeed the physiologically relevant timescale (Schneiderman & Gormezano, 1964). Furthermore, the cerebellum seems to be critically involved in the acquisition and performance of the timed response (McCormick, Clark, Lavond, & Thompson, 1982; Perret, Ruiz, & Mauk, 1993; Yeo & Hesslow, 1998; Ahn & Welsh, 1999). The described mechanism provides a new explanation for how the cerebellar network can solve timing tasks on a timescale that is almost two orders of magnitude larger than the

millisecond timescale usually attributed to neuronal dynamics (Kistler & van Hemmen, 1999; Kistler et al., 2000).

In reality, time is a continuous variable, and therefore sources of noise other than synaptic transmission failures come into play—noise in the timing of action potentials, nonperfect synchronization, or heterogeneously distributed delays in the reverberating loop. In order to address these issues, we developed in section 3 a conductance-based network model for a population of IO neurons. This model can exactly reproduce the spike patterns of the (noise-free) time-discrete model, at least as long as a narrow distribution of delays in the reverberating loop is used. The assumptions on synchrony and rhythmicity implicitly made in the time-discrete model are thus confirmed; neurons stay synchronized, though only a subpopulation is active during each cycle. The mechanisms that keep the population synchronized—common synaptic input and electrotonic coupling—are well understood and studied elsewhere (Gerstner et al., 1996; Chow & Kopell, 2000).

In the context of the olivo-cerebellar system, timing issues might actually be more important than transmission failures because some of the involved synapses, such as the climbing fiber-Purkinje cell synapses, seem to be particularly suitable for a reliable transmission of action potentials. Nevertheless, the dense coupling of IO neurons via gap junctions indicates that nature has taken care to keep IO neurons well synchronized. Simulations of the conductance-based network model show that the strength of the electrotonic coupling is a delicate issue. If the coupling is too strong, then synaptic input will no longer trigger only the postsynaptic neuron but a whole bunch of electrotonically coupled cells. On the other hand, if the coupling is too weak, then spikes within one cycle are only poorly synchronized. The coupling finally used in the simulations presented in Figures 13 through 15 is in keeping with a rather weak coupling of IO cells in rat (Devor & Yarom, 2001).

In this article, we have studied the olivo-cerebellar system. The general principle of a dynamical working memory, however, can carry over to other structures of the brain. Thalamic relay neurons, for instance, provide another example of neurons that show postinhibitory rebound and thus form a potential substrate for a delayed triggering of action potentials. These neurons are embedded in topographically organized loops that reciprocally connect the thalamic nuclei with the cerebral cortex (Sherman & Koch, 1990; Billock, 1997). Similarities with the loops connecting inferior olive and cerebellar cortex are not necessarily coincidental.

Appendix: Conductance-Based Network Model

The simulations presented in section 3 are based on a model of inferior olivary neurons developed by Schweighofer et al. (1999). We have adapted this model as follows.

In order to account for the co-location of synapses and gap junctions in dendritic glomeruli, we have added an extra dendritic compartment to the original two-compartment model. The somatic compartment and the (large) dendritic compartment are equipped with the same set of ion channels as in the model of Schweighofer et al. (1999). The parameter values are $g_{\mathrm{Na}} = 70$, $g_{\mathrm{K\_dr}} = 22$, $g_{\mathrm{Ca\_l}} = 0.75$, $g_{\mathrm{h}} = 1.5$, $g_{\mathrm{Ca\_h}} = 4$, $g_{\mathrm{K\_Ca}} = 35$, $g_{\mathrm{ls}} = g_{\mathrm{ld}} = 0.015$ (all conductances in mS/cm^2). The morphology of the somatic and the large dendritic compartment corresponds to the "standard cell" of Schweighofer et al. (1999)—$g_{\mathrm{int}} = 0.13$ mS/cm^2 and $p = 0.2$ with a total area of 10,000 μm^2. The extra compartment, which contains gap junctions and synaptic conductances, is connected to the soma and is supposed to represent a single (passive) dendrite with a length of 100 μm and radius 0.6 μm.

Gap junctional coupling within the network is assumed to be all-to-all, in keeping with the experimental result that each IO neuron is coupled to 10 to 40 neighboring cells (Devor & Yarom, 2001). The current through a gap junction is described as in the original model with a conductivity of $g_{\mathrm{c}} = 0.5$ nS which results in a coupling coefficient of about 0.1 similar to values reported by Devor and Yarom (2001).

Synaptic input is described by the activation of time-dependent conductances in the extra compartment. The synaptic current is of the form

$$I_{\mathrm{syn}}(t) = g[v(t) - E]S \times \left(\sum_i \left[\mathrm{e}^{-(t-t_i)/\tau_2} - \mathrm{e}^{-(t-t_i)/\tau_1} \right] \Theta(t - t_i)/c_{\tau_1,\tau_2} \right). \tag{A.1}$$

Here, the sum is over all arrival times t_i of presynaptic action potentials, Θ is the Heaviside step function, c_{τ_1,τ_2} is a constant that normalizes the height of the peak of $\mathrm{e}^{-(t-t_i)/\tau_2} - \mathrm{e}^{-(t-t_i)/\tau_1}$ to unity, and g is the peak conductance. $S(x) = (1 - \exp[-x/k])/(1 - \exp[-1/k])$ with $k = 2$ is a saturating function that describes a sublinear superposition of postsynaptic currents that have been triggered by simultaneously arriving presynaptic spikes. GABAergic synapses are modeled by a raise time of $\tau_1 = 0.5$ ms, an exponential decay with time constant $\tau_2 = 20$ ms, and a reversal potential of $E = -75$ mV. AMPA sensitive synapses have $\tau_1 = 0.5$ ms, $\tau_2 = 2$ ms, and $E = 0$ mV.

The resulting (440-dimensional) differential equation is solved by custom-made software based on a modified Bulirsch-Stoer integration scheme (Press, Teukolsky, Vetterling, & Flannery, 1992). One second of real time requires about 15 to 30 minutes CPU time on a 800 MHz PIII Linux PC.

Acknowledgments

Part of this work was completed during a visit of W. M. K. at the Hebrew University of Jerusalem, and it is his great pleasure to thank Idan Segev and Yosef Yarom for their hospitality. We also thank Moritz Franosch, Christian

Leibold, and Oliver Wenisch from the group of Leo van Hemmen, Technical University of Munich, for computing time on some of their Linux PCs. W. M. K. is supported by the NWO-Pioneer Program to C. I. De Zeeuw.

References

Ahn, E. S., & Welsh, J. P. (1999). Inferior olive optimizes but is not required for associative learning as measured by eyeblink conditioning. *Soc. Neurosci. Abstr., 25*, 1560.

Aizenman, C. D., & Linden, D. J. (1999). Regulation of the rebound depolarization and spontaneous firing patterns of deep nuclear neurons in slices of rat cerebellum. *J. Neurophysiol., 82*, 1697–1709.

Aizenman, C. D., Manis, P. B., & Linden, D. J. (1998). Polarity of long-term synaptic gain change is related to postsynaptic spike firing at a cerebellar inhibitory synapse. *Neuron, 21*, 827–835.

Amit, D. J. (1989). *Modeling brain function—the world of attractor neural networks*. Cambridge: Cambridge University Press.

Armstrong, D. M., Cogdell, B., & Harvey, R. J. (1975). Effects of afferent volleys from the limbs on the discharge patterns of interpositus neurones in cats anaesthetized with α-chloralose. *J. Physiol. (Lond.), 248*, 489–517.

Armstrong, D. M., Cogdell, B., & Harvey, R. J. (1979). Discharge patterns of Purkinje cells in cats anaesthetized with α-chloralose. *J. Physiol. (Lond.), 291*, 351–366.

Ash, R. (1990). *Information theory*. New York: Dover.

Bal, T., & McCormick, D. A. (1997). Synchronized oscillations in the inferior olive are controlled by the hyperpolarization-activated cation current I_h. *J. Neurophysiol., 77*, 3145–3156.

Bell, C. C., & Kawasaki, T. (1972). Relations among climbing fiber responses of nearby Purkinje cells. *J. Neurophysiol., 35*, 155–169.

Billock, V. A. (1997). Very short-term visual memory via reverberation: A role for the cortico-thalamic excitatory circuit in temporal filling-in during blinks and saccades? *Vision Res., 37*, 949–953.

Boylls, C. C. (1978). Prolonged alterations of muscle activity in locomoting premammiliary cats by microstimulation of the inferior olive. *Brain Res., 159*, 445–450.

Brunel, N. (2000). Dynamics of sparsely connected networks of excitatory and inhibitory spiking neurons. *J. Comput. Neurosci., 8*, 183–208.

Chow, C. C., & Kopell, N. (2000). Dynamics of spiking neurons with electrical coupling. *Neural Comput., 12*, 1643–1678.

Crick, F. (1994). *The astonishing hypothesis*. New York: Scribner.

Crisanti, A., & Sompolinsky, H. (1988). Dynamics of spin systems with randomly asymmetric bonds: Ising spins and Glauber dynamics. *Phys. Rev. A, 37*, 4865–4874.

Czubayko, U., Sultan, F., Thier, P., & Schwarz, C. (2001). Two types of neurons in the rat cerebellar nuclei as distinguished by membrane potentials and intracellular fillings. *J. Neurophysiol., 85*, 2017–2029.

Deans, M. R., Gibson, J. R., Sellitto, C., Connors, B. W., & Paul, D. L. (2001). Synchronous activity of inhibitory networks in neocortex requires electrical synapses containing connexin36. *Neuron, 31*, 477–485.

Derrida, B., Gardner, E., & Zippelius, A. (1987). An exactly solvable asymmetric neural network model. *Europhys. Lett., 2*, 167–173.

Desclin, J. C. (1974). Histological evidence supporting the inferior olive as the major source of cerebellar climbing fibers in the cat. *Brain Res., 77*, 365–384.

Devor, A., & Yarom, Y. (2001). *Electrotonic coupling in the inferior olivary nucleus revealed by simultaneous double patch recordings*. Unpublished.

De Zeeuw, C. I., Lang, E. J., Sugihara, I., Ruigrok, T. J. H., Eisenman, L. M., Mugnaini, E., & Llinás, R. (1996). Morphological correlates of bilateral synchrony in the rat cerebellar cortex. *J. Neurosci., 16*, 3412–3426.

De Zeeuw, C., & Ruigrok, T. J. (1994). Olivary projecting neurons in the nucleus of Darkschewitsch in the cat receive excitatory monosynaptic input from the cerebellar nuclei. *Brain Res., 653*, 345–350.

De Zeeuw, C. I., Simpson, J. I., Hoogenraad, C. C., Galjart, N., Koekkoek, S. K. E., & Ruigrok, T. J. H. (1998). Microcircuitry and function of the inferior olive. *Trends Neurosci., 21*, 391–400.

De Zeeuw, C., Wylie, D. R., Digiorgi, P. L., & Simpson, J. I. (1994). Projections of individual Purkinje cells of identified zones in the flocculus to the vestibular and cerebellar nuclei in the rabbit. *J. Comp. Neurol., 349*, 428–447.

Fusi, S., Del Giudice, P., & Amit, D. J. (2000). Neurophysiology of a VLSI spiking neural network: LANN21. In S. Amari, C. L. Giles, & V. Piuri (Eds.), *Neural computing: New challenges and perspectives for the new millennium*. Piscataway, NJ: IEEE Computer Society Press.

Gerstner, W., van Hemmen, J. L., & Cowan, J. D. (1996). What matters in neuronal locking? *Neural Comput., 8*, 1689–1712.

Güldenagel, M., Ammermüller, J., Feugenspan, A., Teubner, B., Degen, J., Söhl, G., Willecke, K., & Weiler, R. (2001). Visual transmission deficits in mice with targeted disruption of the gap junction gene connexin36. *J. Neurosci, 21*, 6036–6044.

Hopfield, J. J. (1982). Neural networks and physical systems with emergent collective computational abilities. *Proc. Natl. Acad. Sci. USA, 79*, 2554–2558.

Hormuzdi, S. G., Pais, I., LeBeau, F. E. N., Towers, S. K., Rozov, A., Buhl, E. H., Whittington, M. A., & Monyer, H. (2001). Impaired electrical signaling disrupts gamma frequency oscillations in connexin36-deficient mice. *Neuron, 31*, 487–495.

Ito, M. (1984). *The cerebellum and neural control*. New York: Raven Press.

Jahnsen, H. (1986). Electrophysiological characteristics of neurones in the guinea-pig deep cerebellar nuclei in vitro. *J. Physiol. (Lond.), 372*, 129–147.

Kirkpatrick, S., & Sherrington, D. (1978). Infinite-ranged models of spinglasses. *Phys. Rev. B, 17*, 4384–4403.

Kistler, W. M., & van Hemmen, J. L. (1999). Delayed reverberation through time windows as a key to cerebellar function. *Biol. Cybern., 81*, 373–380.

Kistler, W. M., van Hemmen, J. L., & De Zeeuw, C. I. (2000). Time window control: A model for cerebellar function based on synchronization, reverberation, and time slicing. In N. M. Gerrits, T. J. H. Ruigrok, and C. I. De Zeeuw

(Eds.), *Cerebellar modules: Molecules, morphology, and function* (pp. 275–297). Amsterdam: Elsevier.

Kree, R., & Zippelius, A. (1991). Asymmetrically diluted neural networks. In E. Domany, J. L. van Hemmen, & K. Schulten (Eds.), *Models of neural networks*. Berlin: Springer-Verlag.

Lampl, I., & Yarom, Y. (1993). Subthreshold oscillations of the membrane potential: A functional synchronizing and timing device. *J. Neurophysiol., 70*, 2181–2186.

Lang, E. J. (2001). Organization of olivocerebellar activity in the absence of excitatory glutamatergic input. *J. Neurosci., 21*, 1663–1675.

Lang, E. J., Sugihara, I., & Llinás, R. (1996). GABAergic modulation of complex spike activity by the cerebellar nucleoolivary pathway in rat. *J. Neurophysiol., 76*, 255–275.

Lang, E. J., Sugihara, I., Welsh, J. P., & Llinás, R. (1999). Patterns of spontaneous Purkinje cell complex spike activity in the awake rat. *J. Neurosci., 19*, 2728–2739.

Llinás, R., & Mühlethaler, M. (1988). Electrophysiology of guinea-pig cerebellar nuclear cells in the in vitro brain stem–cerebellar preparation. *J. Physiol. (Lond.), 404*, 241–258.

Llinás, R., & Sasaki, K. (1989). The functional organization of the olivocerebellar system as examined by multiple Purkinje cell recordings. *Eur. J. Neurosci., 1*, 587–602.

Llinás, R., & Yarom, Y. (1986). Oscillatory properties of guinea-pig inferior olivary neurones and their pharmacological modulation: An *in vitro* study. *J. Physiol. (Lond.), 376*, 163–182.

Loewenstein, Y., Yarom, Y., & Sompolinsky, H. (2000). Complex spikes and bursting activity of simple spikes of cerebellar Purkinje cells are highly correlated. *Neurosci. Lett., 55*, 35.

Maass, W., Natschläger, T., & Markram, H. (in press). Real-time computing without stable states: A new framework for neural computation based on perturbations. *Neural Computation*.

McCormick, D. A., Clark, G. A., Lavond, D. G., & Thompson, R. F. (1982). Initial localization of the memory trace for a basic form of learning. *Proc. Natl. Acad. Sci. USA, 79*, 2731–2735.

McCulloch, W. S., & Pitts, W. (1943). A logical calculus of ideas immanent in nervous activity. *Bulletin of Mathematical Biophys., 5*, 115–133.

Nützel, K. (1991). The length of attractors in asymmetric random neural networks with deterministic dynamics. *J. Phys. A: Math. Gen., 24*, L151–L157.

Nützel, K., Kien, J., Bauer, K., Altman, J. S., & Krey, U. (1994). Dynamics of diluted attractor neural networks with delays. *Biol. Cybern., 70*, 553–561.

Perret, S. P., Ruiz, B. P., & Mauk, M. D. (1993). Cerebellar cortex lesions disrupt learning-dependent timing of conditioned eyelid response. *J. Neurosci., 13*, 1708–1718.

Press, W. H., Teukolsky, S. A., Vetterling, W. T., & Flannery, B. P. (1992). *Numerical recipes in C* (2nd ed.). Cambridge: Cambridge University Press.

Rash, J. E., Staines, W. A., Yasumura, T., Patel, D., Furman, C. S., Stelmack, G. L., & Nagy, J. I. (2000). Immunogold evidence that neuronal gap junctions in adult brain and spinal cord contain connexin-36 but not connexin-32 or connexin-43. *Proc. Natl. Acad. Sci. USA, 97*, 7573–7578.

Ruigrok, T. J. H. (1997). Cerebellar nuclei: The olivary connection. In C. I. De Zeeuw & J. Voogd (Eds.), *Progress in brain research* (Vol. 114, pp. 167–192). Amsterdam: Elsevier Science.

Schneiderman, N., & Gormezano, I. (1964). Conditioning of the nictitating membrane response of the rabbit as a function of CS-US interval. *J. Comp. Physiol. Psychol., 57*, 188–195.

Schweighofer, N., Doya, K., & Kawato, M. (1999). Electrophysiological properties of inferior olive neurons: A compartmental model. *J. Neurophysiol., 82*, 804–817.

Shadlen, M. N., & Newsome, W. T. (1994). Noise, neural codes and cortical organization. *Current Opinion in Neurobiology, 4*, 569–579.

Sherman, S. M., & Koch, C. (1990). Thalamus. In G. Shepherd (Ed.), *The synaptic organization of the brain* (pp. 246–278). New York: Oxford University Press.

Softky, W., & Koch, C. (1993). The highly irregular firing pattern of cortical cells is inconsistent with temporal integration of random EPSPS. *J. Neurosci., 13*, 334–350.

Sotelo, C., Llinás, R., & Baker, R. (1974). Structural study of inferior olivary nucleus of the cat: Morphological correlations of electrotonic coupling. *J. Neurophysiol., 37*, 541–559.

Szentagothai, J., & Rajkovits, K. (1959). Über den Ursprung der Kletterfasern des Kleinhirns. *Z. Anat. Entwickl. Gesch., 121*, 130–141.

Treves, A., & Panzeri, S. (1995). The upward bias in measures of information derived from limited data samples. *Neural Comput., 7*, 399–407.

van Vreeswijk, C., & Sompolinsky, H. (1998). Chaotic balanced state in a model of cortical circuits. *Neural Comput., 10*, 1321–1371.

Yeo, C. H., & Hesslow, G. (1998). Cerebellum and conditioned reflexes. *Trends Cognit. Sci., 2*, 322–330.

Received July 5, 2001; accepted April 30, 2002.

This article has been cited by:

2. F. E. Hoebeek, L. Witter, T. J. H. Ruigrok, C. I. De Zeeuw. 2010. Differential olivo-cerebellar cortical control of rebound activity in the cerebellar nuclei. *Proceedings of the National Academy of Sciences* **107**:18, 8410-8415. [CrossRef]
3. Mikhail I. Rabinovich, Ramón Huerta, Pablo Varona, Valentin S. Afraimovich. 2006. Generation and reshaping of sequences in neural systems. *Biological Cybernetics* **95**:6, 519-536. [CrossRef]
4. Mikhail Rabinovich, Pablo Varona, Allen Selverston, Henry Abarbanel. 2006. Dynamical principles in neuroscience. *Reviews of Modern Physics* **78**:4, 1213-1265. [CrossRef]
5. Julien Mayor, Wulfram Gerstner. 2005. Signal buffering in random networks of spiking neurons: Microscopic versus macroscopic phenomena. *Physical Review E* **72**:5. . [CrossRef]
6. Naoki Masuda , Brent Doiron , André Longtin , Kazuyuki Aihara . 2005. Coding of Temporally Varying Signals in Networks of Spiking Neurons with Global Delayed FeedbackCoding of Temporally Varying Signals in Networks of Spiking Neurons with Global Delayed Feedback. *Neural Computation* **17**:10, 2139-2175. [Abstract] [PDF] [PDF Plus]
7. Goran Söhl, Stephan Maxeiner, Klaus Willecke. 2005. Expression and functions of neuronal gap junctions. *Nature Reviews Neuroscience* **6**:3, 191-200. [CrossRef]